

Measuring and Controlling the Spectral Bias for Self-Supervised Image Denoising

^{1st} Wang Zhang, Huaqiu Li*
Tsinghua University

^{2nd} Xiaowan Hu
Tsinghua University

^{3rd} Tao Jiang
Tsinghua University

^{4nd} Zikang Chen
Tsinghua University

Haoqian Wang†
Tsinghua University

Abstract—Current self-supervised denoising methods for paired noisy images typically involve mapping one noisy image through the network to the other noisy image. However, after measuring the spectral bias of such methods using our proposed Image Pair Frequency-Band Similarity, it suffers from two practical limitations. Firstly, the high-frequency structural details in images are not preserved well enough. Secondly, during the process of fitting high frequencies, the network learns high-frequency noise from the mapped noisy images. To address these challenges, we introduce a Spectral Controlling network (SCNet) to optimize self-supervised denoising of paired noisy images. First, we propose a selection strategy to choose frequency band components for noisy images, to accelerate the convergence speed of training. Next, we present a parameter optimization method that restricts the learning ability of convolutional kernels to high-frequency noise using the Lipschitz constant, without changing the network structure. Finally, we introduce the Spectral Separation and low-rank Reconstruction module (SSR module), which separates noise and high-frequency details through frequency domain separation and low-rank space reconstruction, to retain the high-frequency structural details of images. Experiments performed on synthetic and real-world datasets verify the effectiveness of SCNet. The code will be released soon.

Index Terms—Self-supervised denoising Spectral controlling network Frequency-band similarity High-frequency structural details Low-rank reconstruction

I. INTRODUCTION

Image denoising is a fundamental task in low-level image processing, aiming to remove noise and restore clean images. Image sensors introduce various types of noise such as thermal, photon, and dark current due to factors like the working environment and electronic components. Importance of image denoising lies in visual applications, where the quality of denoising significantly impacts the performance of downstream tasks such as super-resolution [1], semantic segmentation [2], and object detection [3]. With the advance of neural networks, supervised denoising methods, such as DnCNN [3], NBNNet [4], and NAFNet [5], have proven effective in removing noise. However, these methods rely on large quantities of high-quality noisy-clean image pairs. To address the dependency on high-quality noisy/clean image pairs, self-supervised methods have emerged to circumvent the constraints of paired data. DIP [6] developed methods that learn deep priors from a single noisy image. Masking methods such as [7]–[11], avoid the complexities associated with training using a single

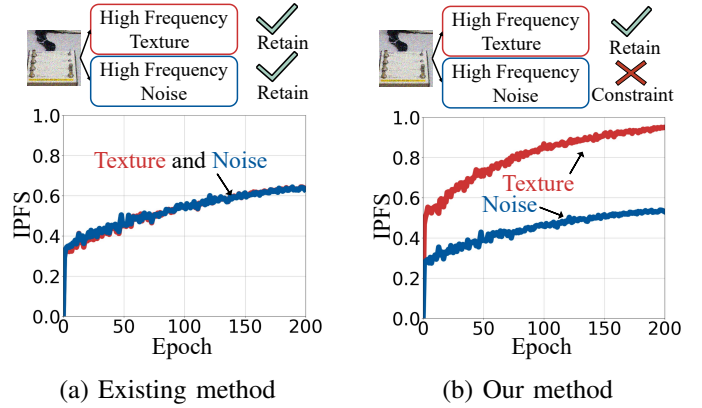


Fig. 1: Comparison between existing self-supervised denoising methods and our methods in high frequency. Our method can selectively suppress high-frequency noise while preserving high-frequency texture details.

image. However, due to the large blind spots in the input, the receptive field for predicting pixels loses a significant amount of valuable context, leading to poorer performance. Noise2Noise (N2N) [12], which theoretically suggests that clean image pairs are not necessary for training, indicates that training solely on noisy images can yield results comparable to those obtained from noisy-clean image pairs. The practical implementation of N2N requires multiple noisy samples of the same scene, which presents challenges in real-world scenarios. LD-RPS [13] utilizes the diffusion prior to generate restored image, while ignoring the frequency loss. NBR2NBR and Prompt-SID [14], [15] addresses this challenge by generating sub-image pairs from downsampled versions of the original image. However, these methods that utilize image pairs do not address the spectral bias of the denoising network. CRnet [16] enhances image quality by unifying restoration. In the unsupervised domain, MCSB [17] optimizes image restoration with Deep Image Prior (DIP) by controlling the frequency. However, it only works for single image.

As shown in Figure 1(a), existing methods fail to consider the heterogeneity between high-frequency noise and details when addressing spectral bias, leading the network to treat all high-frequency signals equally, which is detrimental to image content restoration. In contrast, the method presented in Figure 1(b) effectively addresses this shortcoming. Our approach selectively constrains high-frequency noise in the

These authors contributed equally.

Haoqian Wang is corresponding author. wanghaoqian@tsinghua.edu.cn

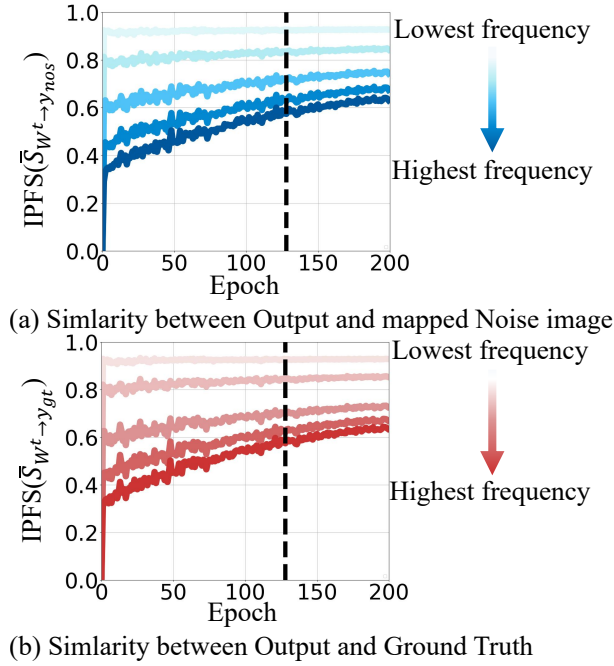


Fig. 2: Spectrum measurement of paired noisy images during network iteration in the existing method. (a) represents the frequency band similarity between the output and the mapped noisy image; (b) represents the frequency band similarity between the output and the ground truth (GT). The peak value of PSNR is indicated by the dashed line.

frequency domain while preserving high-frequency textures, resulting in high-quality self-supervised denoising.

II. MOTIVATION

In this work, we demonstrate that the frequency-domain learning capability of the network is crucial for optimizing self-supervised denoising of paired noisy images, which are generated by down-sampling from NBR2NBR. We achieve this by using a metric called Image Pair Frequency-band Similarity (IPFS), which provides spectral measurements between output and mapped noisy images and between output and ground truth images in self-supervised denoising of paired noisy images. The result is shown in Figure 2.

The proposed metric IPFS examines the input-output similarity of multiple frequency bands in the training of NBR2NBR. The calculation of this metric is similar to the Frequency-Band Correspondence (FBC) metric in MCSB [17]. However, our metric measures the frequency band similarity between the network output and the mapped noisy image, as well as between the network output and the ground truth.

As depicted in Figure 2, the frequency band similarity between the network output and the mapped noisy image shows that during the network’s iterative process, the similarity of low-frequency components reaches its peak initially. In contrast, the similarity of high-frequency components continues to rise throughout the entire iteration process. During the iterative process, when the network reaches the highest PSNR point, the

similarity of high-frequency components between the network output and the ground truth of the noisy images continues to increase while the PSNR does not improve further. At the same time, the similarity of high-frequency components between the network output and the mapped noisy images also continues to increase.

In conclusion, the key to improving the self-supervised denoising effect of paired noisy images is to enhance the network’s ability to retain structures of high-frequency signals and constraint the fitting of high-frequency noise. In this paper, we propose an end-to-end self-supervised denoising framework named SCNet. The main contributions can be summarized as follows:

- We suggest choosing images with more high-frequency components as the denoised images pass through the network to enhance the network’s ability to extract high-frequency image details and accelerate convergence.
- We propose a self-supervised approach to denoising achieved by controlling the learning rate for high-frequency noisy signals from a new parameter optimization perspective by limiting the Lipschitz constant of convolutional layers.
- To retain high-frequency structured textures, we introduce a Spectral Separation and low-rank space Reconstruction module (SSR module). It can be flexibly integrated into the network and separates high-frequency structural information from noise by performing frequency-domain separation and reconstruction.
- Compared to state-of-the-art methods on widely used synthetic and real-image denoising benchmarks, our method delivers highly competitive results.

III. METHOD

In this section, we will provide a detailed description of the workflow for the self-supervised denoising Spectral Control Network (Figure 3) we proposed.

A. Overall Architecture

As is shown in Figure 3(a), our SCNet adopts the simple U-Net architecture as the baseline. We first propose a Frequency Selection Decision (FSD), which suggests that noisy images passing through the network should be selectively chosen in the frequency domain. Then, we uniformly restrict the network’s learning capability for high-frequency signals by controlling the Lipschitz constant of the convolutional kernels, aiming to maximize the denoising effect in the frequency domain. Finally, to supplement and preserve high-frequency texture information, we use the SSR module to separate textures and noise and retain high-frequency texture details between the upstream and downstream of the network.

The proposed Frequency Selection Decision (Figure 3(b)) is a frequency domain selection decision for paired noisy images. We first calculate the high-frequency components of the two noisy images and designate those images with more high-frequency signals to pass through the network for denoising.

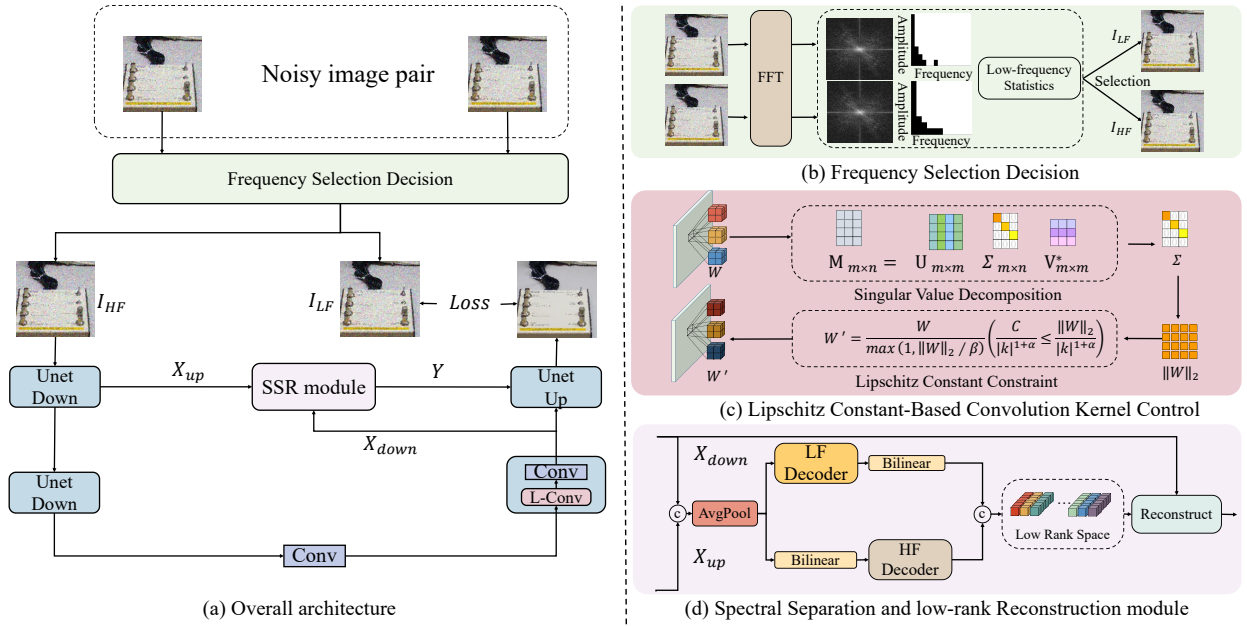


Fig. 3: (a) Overall architecture of the SCNet. (b) Perform frequency domain selection on noisy image pairs using FSD. (c) Control convolutional layers to constrain high-frequency noise by using the Lipschitz constant. (d) Separate and reconstruct high-frequency details by using the SSR module.

This method helps improve the network’s ability to extract high-frequency information.

B. Lipschitz Control for Convolution Kernels

From a frequency domain perspective, noise is predominantly present in high frequencies, and the network tends to fit high-frequency noise in the later stages of iteration. This problem can be mitigated by adjusting the spectrum of learnable layers, as shown in Figure 3(c), to control the learning rate of these high-frequency signals, we constrain the Fourier coefficients of the learnable layers (i.e., convolutional layers) by limiting the network’s Fourier spectrum. Specifically, We assume that the convolutional layers in our network are Lipschitz continuous. This means that the rate at which the network’s output changes in response to its input does not exceed a fixed rate L . Formally, for any arbitrary input x_1 and x_2 , the output $f(x_1)$ and $f(x_2)$ satisfies the following condition:

$$\|f(x_1) - f(x_2)\| \leq L\|x_1 - x_2\| \quad (1)$$

where L is the Lipschitz constant. This inequality ensures that the output difference is bounded by the input difference scaled by L , indicating that the network’s response to changes in the input is controlled and predictable. The Lipschitz constant C is the smallest value that satisfies the above inequality. It represents the maximum rate at which the function f can change with respect to its input. In other words, C is the smallest bound on the gradient of the function.

The rate of decay of Fourier coefficients is closely related to the smoothness of the function. Smooth functions tend to have Fourier coefficients that decay rapidly, while non-smooth

functions have Fourier coefficients that decay more slowly. For a Lipschitz continuous function, its Fourier coefficients typically satisfy a certain decay condition:

$$\|\hat{f}(k)\| \leq \frac{C}{|k|^{1+\alpha}}, \quad (2)$$

where $\hat{f}(k)$ represents the Fourier coefficient at frequency k , and α is related to the degree of smoothness of the function, the value of α typically ranges from 0 to 1.

Further, the Lipschitz constant of a convolution layer is bounded by the spectral norm of its parameters, which means $C \leq \|W\|_2$. We obtain:

$$\|\hat{f}(k)\| \leq \frac{C}{|k|^{1+\alpha}} \leq \frac{\|W\|_2}{|k|^{1+\alpha}}, \quad (3)$$

where C denotes the Lipschitz constant of the convolution layer and $\|W\|_2$ represents the spectral norm of the weight matrix W of the convolution layer. $\|W\|_2$ can be approximated relatively quickly through a few iterations of the power method within the neural network.

The power law $|k|^{1+\alpha}$ indicates that the spectral decay is more pronounced at higher frequencies, implying that learning higher frequencies necessitates a larger spectral norm. Thus, we can control the ability of convolution kernels to learn higher frequencies by constraining its spectral norm W to $\frac{W}{\max(1, \|W\|_2/\beta)}$ with a value β . Then, we normalize W by $\|W\|_2/\beta$ if the weight matrix W is higher than β .

C. Spectral Separation and low-rank Reconstruction

To retain the high-frequency textures of the original image, we separate the image information into high and low frequency

components, enhancing each separately. Figure 3(d) shows the details of the SSR module.

We propose a simple and efficient method to separate low-frequency and high-frequency regions and to enhance the frequency domain features independently: First, for a feature F , we use average pooling to downsample it, thereby extracting its low-frequency features $F_{low}^{B \times C \times \frac{H}{2} \times \frac{W}{2}}$.

Secondly, we use bilinear interpolation to upsample F_{low} to the original dimensions $B \times C \times H \times W$. Then, by subtracting these upsampled features from the original features, we obtain the high-frequency information of the original feature, denoted as F_{high} . where Upsample refers to the up-sampling operation using bilinear interpolation. Finally, we upsample the decoded low-frequency features and concatenate them with the decoded high-frequency information to generate the basis vectors for the image's low-rank space.

1) *Low-Rank Space Reconstruction.*: For the generation of the low-rank space and the reconstruction of high-frequency signals there are two steps. Take two feature maps of the same dimensions from both the upstream and downstream of the network, derived from the same image, denoted as X_{up} and X_{down} , and concatenate them to generate the basis extraction vector $X_E \in \mathbb{R}^{B \times C \times H \times W}$. The low-rank basis vector Generator for reconstruction: $G_\theta : \mathbb{R}^{B \times C \times H \times W} \rightarrow \mathbb{R}^{B \times k \times N}$ be a function parameterized by θ can denoted as:

$$v_1, v_2, \dots, v_k = G_\theta(X_E), \quad (4)$$

where X_E is a feature map derived from the high-frequency enhancement module, and v_1, v_2, \dots, v_k be the k low-rank basis vectors. We define a function G_θ implemented by a convolutional block. We input X_E into a simple convolutional block with k output channels to obtain k low-rank basis vectors for the reconstruction of X_{down} .

Since the k basis vectors of the low-rank space generated automatically by the neural network cannot be guaranteed to be orthogonal to each other, an orthogonalization operation is necessary: let matrix $V = [v_1, v_2, \dots, v_k]^T \in \mathbb{R}^{N \times k}$, the column vectors of V represent the basis vectors of the k -dimensional low-rank space $\mathcal{V} \subset \mathbb{R}^N$.

Let $P : \mathbb{R}^N \rightarrow \mathcal{V}$, P can be calculated from V :

$$P = V(V^T V)^{-1} V^T, \quad (5)$$

where the P is the orthogonal projection matrix of the input image in the low-rank space. The normalization term $(V^T V)^{-1}$ is required for orthogonalization.

Then, we use the orthogonal projection matrix P to reconstruct X_{down} in the high-frequency enhanced low-rank space, obtaining a denoised feature map with enhanced high-frequency components, given by:

$$Y = P X_{down}, \quad (6)$$

where the Y is the reconstructed by SSR module from downstream feature map. The reconstruction operations are fully differentiable, thus enabling learning within the network.

IV. EXPERIMENTS

We evaluate our framework on various denoising tasks with both synthetic and real-world noise.

A. Synthetic Noise

Following the setup of previous methods, we selected the ILSVRC2012 [18] validation dataset with image sizes ranging from 256x256 to 512x512 pixels as our validation set. We tested our results on Kodak, BSD300, and Set14, with 10, 3, and 20 iterations respectively, in line with previous experiments. Thus, all methods were evaluated using 240, 300, and 280 individual synthetic noisy images. Specifically, we consider four types of noise in sRGB space: (1) Gaussian noise with $\sigma = 25$, (2) Gaussian noise with $\sigma \in [5, 50]$, (3) Poisson noise with $\lambda = 30$, (4) Poisson noise with $\lambda \in [5, 50]$. As shown in Table I, traditional methods such as BM3D perform worse than deep learning methods, with a significant gap. This indicates that neural networks capture image priors better and fit the distribution of natural images more effectively than traditional handcrafted models. Additionally, other self-supervised denoising methods also demonstrate good denoising results. Despite their effectiveness, they fall significantly short of supervised denoising methods. Our method outperforms model-based or other self-supervised methods both qualitatively and quantitatively. As shown in Figure 4, SCNet demonstrates promising denoising performance across various types of noise. The denoised images are clean and sharp. More importantly, it does not rely on paired data or known noise statistics, highlighting its potential value in applications.

B. Real-world Noise

We further evaluated the performance of our pipeline on the real fluorescence microscopy denoising (FMD) dataset [19]. The noisy microscopy images in this dataset were acquired using commercial confocal, two-photon, and wide-field microscopes. Compared to other methods, our approach demonstrates competitive performance. In particular, our method significantly outperforms self-supervised methods and shows slight improvements over supervised methods (N2C and N2N) in all sub-datasets. We present the quantitative results in Table II. The visual comparisons can be found in Figure 5.

C. Ablation Study

This section conducts an ablation study of the Frequency Selection Decision, Lipschitz method, and SSR module. Note that PSNR(dB)/SSIM is evaluated on the Set14 dataset.

1) *Component Analysis.*: Table III lists the performance of different component. II outperforms I by 0.04 in PSNR and 0.001 in SSIM. From this, it is evident that FSD improves denoising performance. And FSD accelerates convergence by 23 epochs compared to the baseline during training in Synthetic Noise. III outperforms I by 0.13 in PSNR and 0.002 in SSIM, this indicates that Lipschitz method are highly effective. IV outperforms I by 0.32 in PSNR and 0.003 in SSIM, this indicates that SSR preserves and supplements high-frequency texture details. When used after the Lipschitz

Noise Type	Method	KODAK	BSD300	SET14	Noise Type	Method	KODAK	BSD300	SET14
Gaussian $\sigma = 25$	Baseline, N2C	32.43/0.884	31.05/0.879	31.40/0.869	Gaussian $\sigma \in [5, 50]$	Baseline, N2C	32.51/0.875	31.07/0.866	31.41/0.863
	Baseline, N2N	32.41/0.884	31.04/0.878	31.37/0.868		Baseline, N2N	32.50/0.875	31.07/0.866	31.39/0.863
	CBM3D	31.87/0.868	30.48/0.861	30.88/0.854		CBM3D	32.02/0.860	30.56/0.847	30.94/0.849
	Self2Self	31.28/0.864	29.86/0.849	30.08/0.839		Self2Self	31.37/0.860	29.87/0.841	29.97/0.849
	N2V	30.32/0.821	29.34/0.824	28.84/0.802		N2V	30.44/0.806	29.31/0.801	29.01/0.792
	Laine19-mu	30.62/0.840	28.62/0.803	29.93/0.830		Laine19-mu	30.52/0.833	28.43/0.794	29.71/0.822
	Laine19-pme	32.40/0.883	30.99/0.877	31.36/0.865		Laine19-pme	32.40/0.870	30.95/0.861	31.21/0.855
	DBSN	31.64/0.856	29.80/0.839	30.63/0.846		DBSN	30.38/0.826	28.34/0.788	29.49/0.814
	R2R	32.25/0.880	30.91/0.872	31.32/0.865		R2R	31.50/0.850	30.56/0.855	30.84/0.850
	NBR2NBR	32.08/0.879	30.79/0.873	31.09/0.864		NBR2NBR	32.10/0.870	30.73/0.861	31.05/0.858
	Blind2Ublind	32.27/0.880	30.87/0.872	31.27/0.864		Blind2Ublind	32.34/0.872	30.86/0.861	31.14/0.857
	swinIA	30.12/0.819	28.40/0.789	29.54/0.814		swinIA	30.30/0.820	28.40/0.785	29.49/0.809
	DCD-net	32.27/0.881	31.01/0.876	31.29/0.862		DCD-net	32.35/0.872	31.09/0.866	31.09/0.855
	SCNet (Ours)	32.50/0.886	31.19/0.882	31.55/0.871		SCNet (Ours)	32.60/0.878	31.23/0.871	31.54/0.867
Poisson $\lambda = 30$	Baseline, N2C	31.78/0.876	30.36/0.868	30.57/0.858	Poisson $\lambda \in [5, 50]$	Baseline, N2C	31.19/0.861	29.79/0.848	30.02/0.842
	Baseline, N2N	31.77/0.876	30.35/0.868	30.56/0.857		Baseline, N2N	31.18/0.861	29.78/0.848	30.02/0.842
	Anscombe	30.53/0.856	29.18/0.842	29.44/0.837		Anscombe	29.40/0.836	28.22/0.815	28.51/0.817
	Self2Self	30.31/0.857	28.93/0.840	28.84/0.839		Self2Self	29.06/0.834	28.15/0.817	28.83/0.841
	N2V	28.90/0.788	28.46/0.798	27.73/0.774		N2V	28.78/0.758	27.92/0.766	27.43/0.745
	Laine19-mu	30.19/0.833	28.25/0.794	29.35/0.820		Laine19-mu	29.76/0.820	27.89/0.778	28.94/0.808
	Laine19-pme	31.67/0.874	30.25/0.866	30.47/0.855		Laine19-pme	30.88/0.850	29.57/0.841	28.65/0.785
	DBSN	30.07/0.827	28.19/0.790	29.16/0.814		DBSN	29.60/0.811	27.81/0.771	28.72/0.800
	R2R	30.50/0.801	29.47/0.811	29.53/0.801		R2R	29.14/0.732	28.68/0.771	28.77/0.765
	NBR2NBR	31.44/0.870	30.10/0.863	30.29/0.853		NBR2NBR	30.86/0.855	29.54/0.843	29.79/0.838
	Blind2Ublind	31.64/0.871	30.25/0.862	30.46/0.852		Blind2Ublind	31.07/0.857	29.92/0.852	30.10/0.844
	swinIA	29.51/0.805	27.92/0.775	28.74/0.799		swinIA	29.06/0.788	27.74/0.764	28.27/0.780
	DCD-net	31.60/0.870	30.22/0.865	30.41/0.855		DCD-net	31.00/0.857	29.99/0.855	29.99/0.843
	SCNet (Ours)	31.88/0.879	30.55/0.872	30.77/0.861		SCNet (Ours)	31.35/0.865	30.19/0.860	30.48/0.852

TABLE I: Quantitative denoising results on synthetic datasets in sRGB space. The highest PSNR(dB)/SSIM among unsupervised denoising methods is highlighted in **bold**, while the second is underlined.

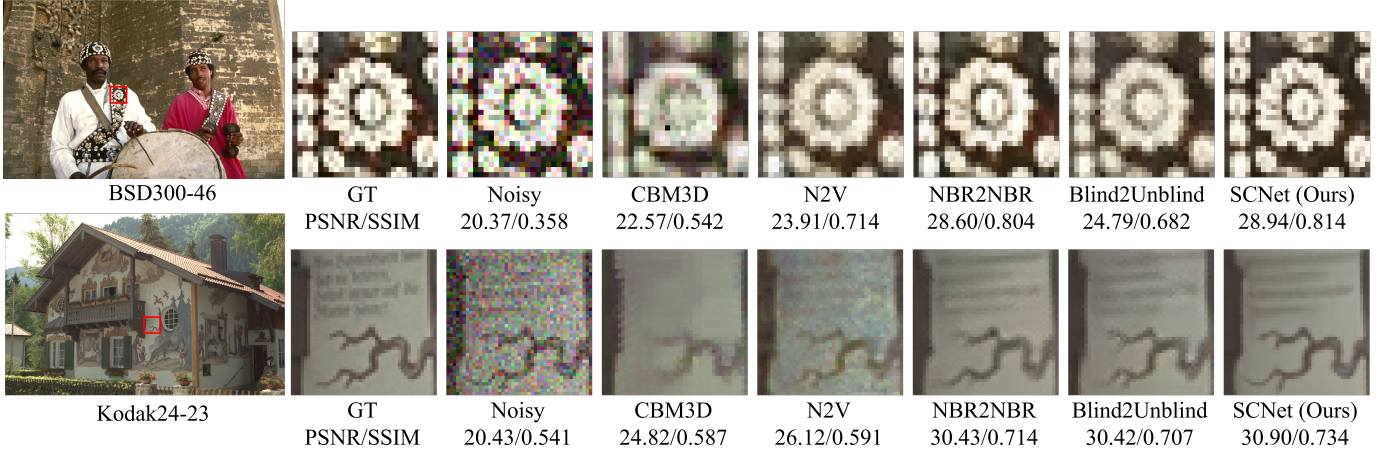


Fig. 4: Visual comparison of denoising sRGB images in the setting of $\sigma = 25$.

method, it further enhances the texture restoration, resulting in a 0.46 dB improvement over the baseline.

2) *High-frequency Denoising of Lipschitz.*: Figure 6 shows the noise suppression capability of the Lipschitz method across the mid, high, and highest frequency bands. It is evident that there is a decrease in similarity with the noisy image by 0.12, 0.11, and 0.10 in these frequency bands, respectively, indicating that the Lipschitz method effectively suppresses the mapping of high-frequency noise.

3) *High-frequency Texture Reconstruction of SSR.*: Figure 7 illustrates the SSR module’s ability to reconstruct frequency domain information during training iterations. It is evident

that the SSR module excels at restoring high-frequency band information, achieving a similarity close to 1 with the ground truth across all frequency bands. This represents a significant improvement compared to the baseline.

V. CONCLUSION

We have demonstrated that the challenge with noisy image pairs lies in separating high-frequency texture details from noise. Based on this conclusion, we propose a new framework that separates high-frequency textures from noise in the frequency domain, addressing the spectral bias in self-supervised denoising. We show the effectiveness and broad

Methods	Confocal Fish	Confocal Mice	Two-Photon Mice
Baseline, N2C	32.79/0.905	38.40/0.966	34.02/0.925
Baseline, N2N	32.75/0.903	38.37/0.965	33.80/0.923
BM3D	32.16/0.886	37.93/0.963	33.83/0.924
N2V	32.08/0.886	37.49/0.960	33.38/0.916
Laine19-mu (G)	31.62/0.849	37.54/0.959	32.91/0.903
Laine19-pme (G)	23.30/0.527	31.64/0.881	25.87/0.418
Laine19-mu (P)	31.59/0.854	37.30/0.956	33.09/0.907
Laine19-pme (P)	25.16/0.597	37.82/0.959	31.80/0.820
NBR2NBR	32.11/0.890	37.07/0.960	33.40/0.921
Blind2Unblind	32.74/0.897	38.44/0.964	34.03/0.916
SCNet (Ours)	33.10/0.910	38.84/0.964	34.16/0.924

TABLE II: Comparison on Confocal Fish, Confocal Mice and Two-Photon Mice. G is for Gaussian and P is for Poisson.

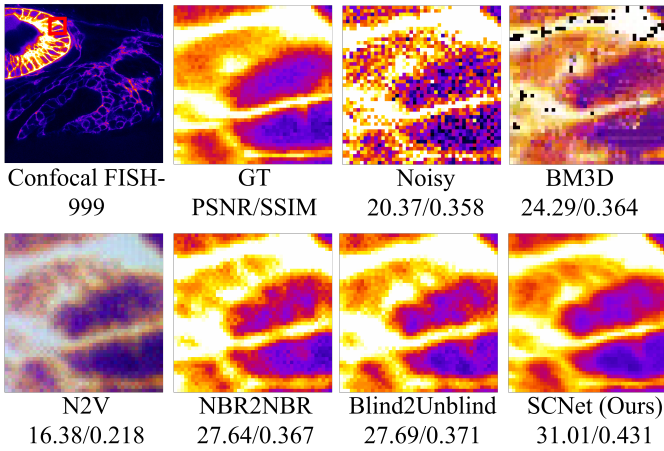


Fig. 5: Visual comparison of denoising FM images.

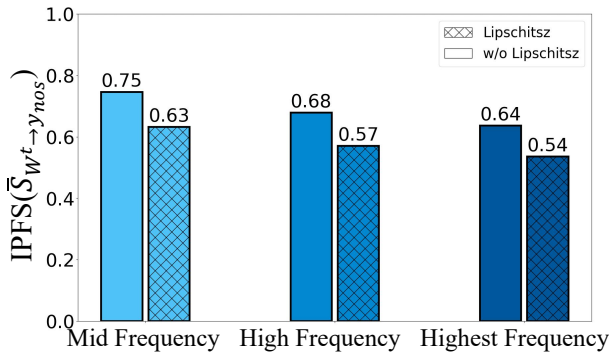


Fig. 6: The denoising performance of the Lipschitz method on top 3 frequency bands ($\bar{S}_{W^{(t)} \rightarrow y_{nos}}$, similarity between the output and the noisy image).

applicability of the proposed SCNet across various denoising tasks involving different noise attributes and data types. We believe this research highlights the advantages of exploring frequency domain processing for self-supervised denoising, offering a new perspective of spectral bias in this field.

method	baseline	FSD	Lipschitz	SSR	PSNR	SSIM
I	✓				31.09	0.864
II	✓	✓			31.13	0.865
III	✓		✓		31.22	0.865
IV	✓			✓	31.41	0.867
V	✓		✓	✓	31.50	0.869
VI	✓	✓	✓	✓	31.55	0.871

TABLE III: Analysis of different component combinations.

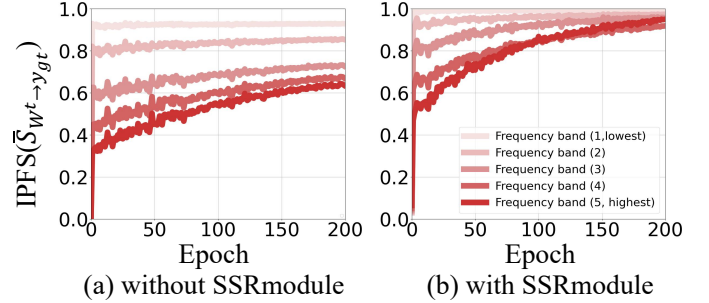


Fig. 7: The restoration performance of the SSR module across all frequency bands ($\bar{S}_{W^{(t)} \rightarrow y_{gt}}$, similarity between the output and the ground truth).

REFERENCES

- [1] Yongqiang Huang, Zexin Lu, Zhimin Shao, Maosong Ran, Jiliu Zhou, Leyuan Fang, and Yi Zhang, "Simultaneous denoising and super-resolution of optical coherence tomography images based on generative adversarial network," *Optics Express*, p. 12289, Apr 2019.
- [2] Ding Liu, Bihan Wen, Jianbo Jiao, Xianming Liu, Zhangyang Wang, and Thomas S. Huang, "Connecting image denoising and high-level vision tasks via deep learning," *IEEE Transactions on Image Processing*, p. 3695–3706, Jan 2020.
- [3] Shijila B., Anju Jose Tom, and Sudhish N. George, "Simultaneous denoising and moving object detection using low rank approximation," *Future Generation Computer Systems*, p. 198–210, Jan 2019.
- [4] Shen Cheng, Yuzhi Wang, Haibin Huang, Donghao Liu, Haoqiang Fan, and Shuaicheng Liu, "Nbnet: Noise basis learning for image denoising with subspace projection," in *2021 IEEE/CVF Conference on Computer Vision and Pattern Recognition (CVPR)*, Jun 2021.
- [5] Liangyu Chen, Xiaojie Chu, Xiangyu Zhang, and Jian Sun, "Simple baselines for image restoration," in *European conference on computer vision*. Springer, 2022, pp. 17–33.
- [6] Victor Lempitsky, Andrea Vedaldi, and Dmitry Ulyanov, "Deep image prior," in *2018 IEEE/CVF Conference on Computer Vision and Pattern Recognition*, Jun 2018.
- [7] Joshua Batson and Loic Royer, "Noise2self: Blind denoising by self-supervision," *arXiv: Computer Vision and Pattern Recognition, arXiv: Computer Vision and Pattern Recognition*, Jan 2019.
- [8] Alexander Krull, Tim-Oliver Buchholz, and Florian Jug, "Noise2void - learning denoising from single noisy images," *Cornell University - arXiv, Cornell University - arXiv*, Nov 2018.
- [9] Huaqiu Li, Xiaowan Hu, and Haoqian Wang, "Interpretable unsupervised joint denoising and enhancement for real-world low-light scenarios," *arXiv preprint arXiv:2503.14535*, 2025.
- [10] Li Huaqiu, Haoqian Wang, et al., "Interpretable unsupervised joint denoising and enhancement for real-world low-light scenarios," in *The Thirtieth International Conference on Learning Representations*, 2025.
- [11] Zikang Chen, Tao Jiang, Xiaowan Hu, Wang Zhang, Huaqiu Li, and Haoqian Wang, "Spatiotemporal blind-spot network with calibrated flow alignment for self-supervised video denoising," in *Proceedings of the AAAI Conference on Artificial Intelligence*, 2025, vol. 39, pp. 2411–2419.

- [12] Jaakko Lehtinen, Jacob Munkberg, Jon Hasselgren, Samuli Laine, Tero Karras, Miika Aittala, and Timo Aila, “Noise2noise: Learning image restoration without clean data,” *International Conference on Machine Learning*, International Conference on Machine Learning, Jan 2018.
- [13] Huaqiu Li, Yong Wang, Tongwen Huang, Hailang Huang, Haoqian Wang, and Xiangxiang Chu, “Ld-rps: Zero-shot unified image restoration via latent diffusion recurrent posterior sampling,” *arXiv preprint arXiv:2507.00790*, 2025.
- [14] Tao Huang, Songjiang Li, Xu Jia, Huchuan Lu, and Jianzhuang Liu, “Neighbor2neighbor: Self-supervised denoising from single noisy images,” in *2021 IEEE/CVF Conference on Computer Vision and Pattern Recognition (CVPR)*, Jun 2021.
- [15] Huaqiu Li, Wang Zhang, Xiaowan Hu, Tao Jiang, Zikang Chen, and Haoqian Wang, “Prompt-sid: Learning structural representation prompt via latent diffusion for single image denoising,” in *Proceedings of the AAAI Conference on Artificial Intelligence*, 2025, vol. 39, pp. 4734–4742.
- [16] Kangzhen Yang, Tao Hu, Kexin Dai, Genggeng Chen, Yu Cao, Wei Dong, Peng Wu, Yanning Zhang, and Qingsen Yan, “Crnet: A detail-preserving network for unified image restoration and enhancement task,” *arXiv preprint arXiv:2404.14132*, 2024.
- [17] Zenglin Shi, Pascal Mettes, Subhransu Maji, and Cees G. M. Snoek, “On measuring and controlling the spectral bias of the deep image prior,” *International Journal of Computer Vision*, p. 885–908, Apr 2022.
- [18] Jia Deng, Wei Dong, Richard Socher, Li-Jia Li, Kai Li, and Li Fei-Fei, “Imagenet: A large-scale hierarchical image database,” in *2009 IEEE conference on computer vision and pattern recognition*. Ieee, 2009, pp. 248–255.
- [19] Yide Zhang, Yinhao Zhu, Evan Nichols, Qingfei Wang, Siyuan Zhang, Cody Smith, and Scott Howard, “A poisson-gaussian denoising dataset with real fluorescence microscopy images,” in *Proceedings of the IEEE/CVF Conference on Computer Vision and Pattern Recognition*, 2019, pp. 11710–11718.